Published in final edited form as:
J Control Release. 2011 December 20; 156(3): 297–306. doi:10.1016/j.jconrel.2011.07.032.

Leveraging the power of ultrasound for therapeutic design and optimization

Charles F. Caskey, PhD, **Xiaowen Hu**, and **Katherine W. Ferrara, PhD**
Department of Biomedical Engineering, University of California, Davis, One Shields Ave, Davis, CA 95616

Abstract

Contrast agent-enhanced ultrasound can facilitate personalized therapeutic strategies by providing the technology to measure local blood flow rate, to selectively image receptors on the vascular endothelium, and to enhance localized drug delivery. Ultrasound contrast agents are micron-diameter encapsulated bubbles that circulate within the vascular compartment and can be selectively imaged with ultrasound. Microbubble transport-based estimates of local blood flow can quantify changes resulting from anti-angiogenic therapies and facilitate differentiation of angiogenic mechanisms. Microbubbles that are conjugated with targeting ligands attach to endothelial surface receptors that are upregulated in disease, providing high signal-to-noise ratio images of pathological vasculature. In addition to imaging applications, microbubbles can be used to enhance localized gene and drug delivery, either by changing membrane and vascular permeability or by carrying and locally releasing cargo. Our goal in this review is to provide an overview of the use of contrast-enhanced ultrasound methodologies in the design and evaluation of therapeutic strategies with emphases on quantitative blood flow mapping, molecular imaging, and enhanced drug delivery.

Keywords

Ultrasound contrast agents; microbubble; targeted drug delivery; molecular imaging; therapeutic ultrasound

1. Introduction

Our goal in this review is to provide an overview of contrast-agent enhanced ultrasound methodologies in the design and application of therapeutic systems. Ultrasound contrast agents are micron-diameter encapsulated bubbles that circulate in the vasculature in a manner similar to erythrocytes; these microbubbles can be selectively imaged with ultrasound. The restriction of intact microbubbles to the intravascular space simplifies the analysis of imaging studies, facilitating quantitation of circulation and accumulation. In this review, we first focus on microbubble imaging, as applied in blood flow estimation and molecular imaging. Second, we detail recent progress in the use of microbubbles to enhance local drug delivery.

Corresponding Author Information: Katherine Ferrara, Department of Biomedical Engineering, University of California, Davis, 451 East Health Sciences Dr., Davis, CA 95616, phone: (530) 754-9436, fax: (530) 754-5739, kwferrara@ucdavis.edu.

The typical microbubble has a core of perfluorocarbon gas and a shell containing a matrix-forming phospholipid and an emulsifying lipid[1]. The shell imparts a barrier between the gas and water for stability and reducing thrombogenic effects *in vivo*. The emulsifying lipid usually contains a polyethelene glycol (PEG) group that is required for efficient production of lipid-coated particles and provides a steric brush that minimizes shell interactions with blood components. Since particle-based imaging and drug delivery systems may be recognized by opsonins and cell-surface receptors and thus removed by the reticuloendothelial system (RES), the presence of a PEG group enhances circulation. The effective emulsifier concentration is limited; exceeding a concentration of 20 mol% 2-kDa PEG can reduce stability [2]whereas reducing the emulsifier concentration or shortening the PEG length can result in coalescence.

The micron-diameter gas core of microbubbles expands and contracts in response to the ultrasound wave, typically expanding slowly and contracting rapidly[3]. As a result of the nonlinear response to the transmitted wave, microbubble-generated sound waves contain frequency components that are multiples and sub-multiples of the driving frequency. Depending on the diameter and on the shell components, a resonance frequency can be defined for each microbubble construct. When driven by ultrasound at a frequency near resonance, microbubble oscillation is efficient and periodic [4]. Further, when driven by a high intensity ultrasound wave, the wall of a microbubble contracts at a velocity of hundreds to thousands of meters per second, and this rapid collapse generates very strong echoes [5].

With rapid collapse due to application of a high ultrasound pressure (~250 kPa or greater), microbubble contrast agents will fragment; the shell can then reform around the bubble fragments to serve as a barrier to passive diffusion, or the remaining gas fragments can diffuse. Fragmentation is often leveraged when microbubbles are applied to quantify blood flow and such techniques are widely used to assess response to therapies, as described in Section 2.

Small molecules, peptides or antibodies are covalently attached to the distal end of PEG for targeting purposes[1]. Such molecularly-targeted agents show great promise to characterize diseases in which vascular receptors are upregulated, pointing the way to effective, individualized therapies; their application is summarized in Section 3. With microbubble collapse near a vessel wall, liquid jets can impinge on the endothelium and disrupt cell membrane integrity. While the generation of liquid jets has been shown to result in holes within cell membranes at high ultrasound intensities, mechanisms responsible for enhanced transport with lower ultrasound intensities are still under investigation[6–8]. Rapid microbubble collapse and associated biological effects facilitate enhanced drug and gene transport and the applications of such techniques are described in Section 4.

2. Parametric imaging of blood flow

Images of intact microbubbles within a target tissue provide estimates of fractional blood volume and contrast agent arrival time[8]. Fragmenting microbubbles locally within a tissue and imaging the replenishment of the vasculature yields local estimates of blood flow. Typically, a gray scale B-mode image is overlaid with a colored parametric map of blood flow, facilitating an understanding of spatial variations in flow in disease or in response to therapy.

In addition to ultrasound, single photon emission computed tomography (SPECT), positron emission tomography (PET), and magnetic resonance imaging (MRI) have been used to quantify blood volume, flow and vascular permeability[9–11]. In particular, SPECT has been routinely utilized to assess myocardial function and regional perfusion in nuclear cardiology [12] and MRI is widely used to assess flow in cancer and cardiovascular

disease[13, 14]. The advantages of ultrasound include the use of an entirely intravascular contrast agent, thus facilitating quantitation, cost, portability and ease of use, and a spatial resolution on the order of hundreds of microns to millimeters.

2.1. Differentiating microbubble from tissue echoes

Traditional B-mode ultrasound creates images of the summed backscatter from both microbubbles and tissue, without discriminating between the two components. Without the use of multiple transmitted pulses, one method to specifically identify microbubble echoes is to use the higher frequency components in microbubble echoes to create images [8]. Alternatively, microbubble-specific imaging techniques can differentiate microbubble and tissue echoes by transmitting pulse sequences that exploit nonlinear changes in microbubble echoes in response to changes in the phase or amplitude of the transmitted pulses. The echoes are then summed algebraically to yield images in which tissue echoes are cancelled and microbubble echoes are summed coherently (Fig. 1) [15–17]. For example, using contrast pulse sequencing (CPS) and the summation of echoes resulting from pulses that were transmitted with phase and amplitude modulation, the contrast agent-to-tissue ratio after summation exceeds 10 times (20 dB) and the image contains little tissue background (Fig. 1b). Using a high frequency scanner (20–50MHz), the spatial resolution of the image improves compared with clinical frequencies (Fig. 1a, 1c); however, some tissue echoes may remain present, although diminished, after pulse summation (Fig. 1c).

2.2. Destruction-replenishment strategy to estimate blood flow

Contrast agent-enhanced ultrasound imaging can be used to detect perfusion defects and follow cardiac wall motion using a destruction-replenishment method[18]. With this method, microbubbles are perfused into the myocardium and then locally fragmented by a high pressure ultrasonic pulse. The mean myocardial microbubble velocity is estimated based on the local replenishment of microbubbles, indicated by a change in video intensity (Fig. 2a). The relationship between the acquired video amplitude, the microbubble replenishment rate (β) and the microvascular cross-sectional area (A) are described by an exponential function, derived by fitting the video amplitude curve to determine the parameters A and β (Fig. 2b). Using this strategy, myocardial perfusion can be visualized, evaluated, [18–20] and correlated with parameters obtained using SPECT [21].

This destruction-replenishment strategy has been applied to clinical applications including cancer [22, 23] (Fig. 2c–e), renal disease [24]and peripheral vascular disease [25]. Tumor blood velocity is typically lower than that of the surrounding tissue; while tumor blood volume can be greater than or less than the surrounding tissue[22]. Microbubble replenishment kinetics can be quantified by using bolus injections as well as continuous infusion, where, following a bolus injection, tumor perfusion based on the A β analysis has been applied to indicate the tumor response to anti-angiogenic drugs[26] (Fig. 2f, g).

Following the local destruction of microbubbles, the time required for replenishment of microbubbles within the region of interest can also be estimated, often termed the “replenishment time” and contrasted with measures of the initial arrival time or washout rate after bolus injection [27]. The advantage of using the replenishment time measure is that this value is insensitive to the effects of gain and attenuation and is easily estimated. The replenishment time measurement has been used to visualize neovascularization in rabbit liver VX2 tumors, resulting in better delineation of tortuous and meandering tumor vessels[28]. Motion-corrected replenishment time estimates have been assigned to a nonlinear color map to easily visualize changes in blood flow in the kidney medulla or cortex with therapy (Fig. 3a, b)[29, 30]. Similarly, the response of rodent tumor vasculature to anti-vascular endothelial growth factor (VEGF) and anti-Activin Like Kinase-1

(ALK-1)therapies has been differentiated by contrasting the effect of these therapies on the replenishment time [31]. Anti-VEGF therapy alters blood flow across a wide range of flow rates and is often interpreted as providing vascular normalization (Fig. 3c, d)[32]. In these studies, the replenishment time derived by ultrasound was correlated with early arrival-time maps acquired with contrast-enhanced MRI [32]. Similarly, ultrasound replenishment time estimates demonstrated that anti-ALK-1 therapy significantly retarded vascular maturation by disrupting the co-localization of endothelial and perivascular cells[31]and thus primarily affected fast replenishment times (Fig. 3e, f).

2.2.1. Other blood flow estimation methods—The pharmacokinetics of contrast agent arrival can also be used to estimate local blood flow without high amplitude ultrasound pulses that fragment microbubbles. The area under the echo amplitude curve and area under the contrast agent wash-out correlate with tumor response and have been routinely used to evaluate new drugs in phase I, II and III clinical trials[33, 34]. The regeneration of the microvasculature can be detected by ultrasound imaging before the morphological changes are detected by computed tomography (CT). Cerebral perfusion deficits have been evaluated by time-to-peak and peak intensity parametric imaging during acute ischemic stroke [35, 36]. Microbubble-based imaging of blood flow complements extracranial and transcranial color-coded duplex sonography in imaging brain perfusion [35, 36]. Brain hemorrhage and glioblastoma with and without large necrotic areas demonstrated different perfusion patterns and such estimates have been shown to change with therapy [37].

3. Molecularly-targeted contrast-enhanced ultrasound

In molecularly targeted ultrasound imaging, microbubbles with covalently conjugated ligands are injected and accumulate at sites where vascular targets have been upregulated. Small molecule ligands are typically attached to a microbubble by coupling the ligand to the lipid prior to particle formation [38]. Attachment of antibodies to preformed microbubbles may be accomplished through the use of a common coupling chemistry, such avidin-biotin, maleimide-thiol or carboxylic acid-amine[1]. We focus here on microbubble contrast agents, although liposomal and perfluorocarbon emulsions have also been used for targeted imaging [39]. This section includes common imaging methods applied in molecular ultrasound imaging and applications of targeted microbubbles.

3.1 Imaging methods for molecularly-targeted ultrasound imaging

The goal of targeted ultrasound imaging is to selectively image microbubbles that are bound to a molecular target on the vascular endothelium, while suppressing signals from surrounding tissues and freely circulating microbubbles. These processes are typically segmented into two parts where differentiation of *microbubble* from *tissue* echoes occurs first, followed by separation of *bound* from *freely circulating microbubble echoes*. Differentiation of microbubbles from tissue was described in Section 2.1.

3.1.1. Differentiating bound from freely-circulating microbubbles—In order to distinguish between *bound* and *freely circulating* microbubble echoes, at least two methods have been developed that build upon the previously discussed microbubble-specific imaging techniques (Fig. 4). Selective imaging of bound microbubbles typically combines sequential data acquired over several minutes to differentiate both between *microbubble* and *tissue* echoes and *bound* and *freely circulating* microbubbles echoes.

Both methods begin with an injection of targeted contrast agents, followed by a delay of several minutes to allow bubbles to circulate and bind to their target. Motion correction and inter-frame image averages can reduce artifacts caused by respiration and signals from

freely circulating microbubbles [40–42]. Once the total microbubble signal reaches a plateau, the method outlined in Fig. 4a uses a high-intensity acoustic burst to destroy bound microbubbles within a local region. Assuming that circulating agents will replenish the region of interest, bound agents are selectively imaged by subtracting the post-burst images (assumed to contain freely-circulating agents) from the pre-burst images (assumed to contain bound and freely-circulating agents). Variations of this technique have been used for many applications (Table 1, "Pre-burst minus post-burst"); however, the high-intensity acoustic pulses may not be desirable for the initial clinical evaluation of targeted microbubbles [43].

An alternative method that does not require a high amplitude destructive pulse to discriminate bound and circulating microbubbles is summarized in Fig. 4b. Here, a 10-second average is acquired at the peak concentration and after 7 minutes and the difference of the later and earlier averaged images is calculated [40]. The inter-frame averaging suppresses echoes from freely circulating microbubbles and with such a strategy the addition of a destructive pulse did not improve the differentiation of bound and circulating agents [40, 44]. Sophisticated processing methods, such as estimation of the spatial frequencies within the targeted image, can also be employed [40].

3.2 Applications

Pre-clinical studies with targeted microbubbles focus on noninvasive imaging of vascular cell-surface receptors with a goal of diagnosing disease or quantifying therapeutic efficacy [45, 46]. The following sections discuss recent pre-clinical studies applying microbubbles targeted to receptors that are upregulated in inflammation and angiogenesis, in applications including cancer, cardiovascular disease and atherosclerosis.

3.2.1. Molecular imaging of angiogenesis—With the advent of drugs targeted to angiogenic receptors on cancerous endothelium, noninvasive assessment of molecular activity is desirable to individualize therapy [47]. The vascular endothelium of tumors undergoing angiogenesis expresses VEGF receptors and integrins which have been successfully targeted with microbubbles conjugated with antibodies, small molecules and peptides (see Table 1, refs [40, 44, 48–56]).

With an array of ligands now available, multi-receptor quantification can be performed to longitudinally profile tumor angiogenesis and monitor therapeutic efficacy. Microbubbles have been targeted to the angiogenesis integrins $\alpha_v\beta_3$ and vascular endothelial growth factor receptor 2 (VEGFR2)using monoclonal antibodies or small molecular ligands (Fig. 3a–e) [40, 48–58]. Within the same imaging study, multiple microbubbles can be sequentially administered and the density of multiple receptors assayed within minutes. Receptors that are upregulated in angiogenesis ($\alpha_v\beta_3$, endoglin, and VEGFR2) have been repeatedly imaged with targeted microbubbles in murine models of breast, ovarian, and pancreatic cancer to profile the longitudinal expression of these receptors (Fig. 5f). Based on ultrasound studies of early stage breast and ovarian cancers, endoglin expression was found to be upregulated before $\alpha_v\beta_3$ integrin and VEGFR2 expression; alternatively, in early stage pancreatic cancer, the difference in expression of these receptors was not significant [54]. Microbubbles targeted to endoglin and VEGFR2 have been applied in pre-clinical studies to follow changes with gemcitabine chemotherapy of pancreatic tumors [44]. Histology and immunohistochemistry suggested that decreases in endoglin and VEGFR2 signals measured by targeted ultrasound were due to decreased vascular density and decreased expression of endoglin and VEGFR2 [44].

3.2.2. Molecular Imaging of inflammation—Pre-clinical studies indicate that ultrasound molecular imaging can detect inflammation associated with atherosclerosis and

track the progression of disease (Table 1[59–64]) [45]. The accumulation of microbubbles targeted to markers for inflammation, vascular cell adhesion molecule-1 (VCAM-1) and P-selectin, was greater in mice deficient for the LDL-receptor and the Apobec-1 editing peptide, as compared to control mice, at ages of 10, 20, and 40 weeks [64]. Evidence of atherosclerotic phenotype was detected prior to the formation of plaques by imaging microbubbles targeted to VCAM-1 and P-selectin [64].

Molecular imaging with ultrasound has been used to image inflammation that occurs after myocardial infarction (Table 1, refs [65, 66])[67]. Microbubbles conjugated to Sialyl Lewis^x can target endothelial P-selectin and increase signal in post-ischemic versus normal myocardium in rats with a surgically induced ischemia-reperfusion injury. These studies concluded that molecular ultrasound may provide a method for increasing diagnostic accuracy of cardiac ischemia [65, 66]. Ultrasound molecular imaging has also been demonstrated to noninvasively image cardiac inflammation [68], Crohn's disease [69], thrombosis [70] and inflammation due to transplant rejection (Table 1) [71].

4. Microbubble- and ultrasound-enhanced drug delivery

Microbubbles have been used to enhance the delivery of genes, proteins and chemotherapeutics in pre-clinical studies [72–74]. Systemic co-injection of a drug-carrying particle and a microbubble, followed by local insonation, has been shown to increase local vascular permeability and allow for the extravasation of the agent [75, 76]. Alternatively, directly incorporating a drug or gene within the shell of the activatable bubble has been shown to locally deliver the drug after insonation [77–79]. Drug-solubilized oils may also be included in the shell to enhance loading [80, 81]. Paclitaxel has been solubilized within an oil coating of the lipid layer and gas core, facilitating the transfer of drugs from the microbubble shell to the endothelium during insonation[82]. Protein and polymer-shelled microbubbles have also been functionalized to carry targeting ligands and genetic payloads [83, 84]. Also, preformed liposomes or other nanoparticles can be conjugated to the membrane, thus enhancing the payload [2, 82, 85]. For example, we find that thousands of small unilamellar liposomes can be attached to a single microbubble without significantly decreasing microbubble oscillation[82]. Hybrid microbubble-liposome vehicles can easily be deflected to the vessel wall by a train of low-pressure ultrasound pulses [2] and the cargo released from the liposomes.

The advantages of microbubbles as drug or gene carriers include enhanced transport across cell membranes and vessel walls resulting from oscillation of the microbubble within tens of microns from the vessel surface (Fig. 6). Hypothesized mechanisms for this enhanced transport include fluid microstreaming as the microbubble oscillates (Fig. 6a), liquid jets directed toward or away from the endothelium (Fig. 6b), transcytosis of particles (Fig. 6c) and the creation of trans-endothelial gaps (Fig. 6d)[7, 8, 86]. The ability to use ultrasound to image, deflect and fragment microbubbles provides local control over when and where a drug is released [86]. The spatial localization of enhanced delivery effects is obtained primarily through positioning of the ultrasound focus. Disadvantages of microbubbles as carriers include the relatively low payload and short circulation half-life, which is on the order of minutes for lipid-shelled vehicles and is extended with polymer-shelled vehicles.

Sub-micron particles that can be activated by ultrasound have also been described, where the smaller diameter of these particles facilitates extravasation from leaky tumor vasculature and targeting to vascular receptors. Liquid perfluorocarbon-containing nanoparticles have been applied for ultrasound and MRI[87, 88], and more recently for therapeutic delivery [89]. Polymer-coated perfluorocarbon nanoparticles can produce an effective cancer therapeutic

when combined with ultrasound [90]. With a stabilizing coating, liquid perfluorocarbons with low phase transition temperatures can be stably incorporated within vehicles.

4.1 Parameters for drug delivery

Critical parameters for quantifying the effects of microbubble oscillation include ultrasound settings, the microbubble diameter and concentration and the vessel diameter[8]. Markers for ultrasound-induced vascular changes that have been used as indications that drug delivery can be enhanced are hemorrhage (extravasation of red blood cells), trans-BBB transport and the extravasation of small imaging probes. The incorporation of targeting ligands is likely to further enhance such effects.

The transmission center frequency (f_o) and the peak rarefactional pressure (PRP) are key parameters in determining the likelihood of biological effects from ultrasound. The mechanical index ($MI=PRP/\sqrt{f_o}$), displayed on all clinical commercial scanners, does not account for the presence of exogenous microbubble agents[91]. Yet, the threshold for cavitation is much lower (MI=0.4) for petechial hemorrhage in gas-containing tissues (eg. lungs) as compared to tissues that do not contain gas bodies[92]. The addition of exogenous agents similarly reduces threshold for bioeffects, and several recent papers have proposed the ratio of acoustic pressure and center frequency (PRP/f_o) as an index that is predictive of the biological effects of microbubble contrast agents [43, 93], where the likelihood of a direct biological effect increases with an increase in this ratio. When ultrasound was applied to the rat kidney with a value of PRP/f_o above 0.5 in the presence of exogenous agents, hemorrhage was detected [43]. The extravasation of fluorescein isothiocyanate (FITC)-labeled dextran from the vasculature increased with PRP/f_o following insonation of microbubbles in the chorioallantoic membrane model [86].

The pulse duration and time between ultrasound pulses are also important factors in the efficiency of drug delivery. Microbubbles repeatedly fragment and re-combine during a long ultrasound pulse and the remaining gas can diffuse over long intervals between pulses. For example, the pressure threshold for blood brain barrier (BBB) disruption decreased from 0.7 to 0.4 MPa when pulse length increased from 0.1 to 10 msec [94]. Similarly, the pressure threshold for disruption of a gel boundary decreased from 2.5 MPa to 1.2 MPa with the pulse duration increasing from 10 μsec to 10 msec [95]. However, when microbubbles are destroyed within the vasculature, sufficient time must be allowed between pulses for the microbubbles to re-enter the vasculature, and therefore a minimum time between pulses must be maintained. In explorations of the effect of the time between pulses, renal hemorrhage decreased with 33 ms between frames, as compared with a 1 second between frames (for a transmitted center frequency of 1.8 MHz, MI of 1.6) [96]. Ten seconds of continuous insonation yielded a similar number of petechial hemorrhages as a 100 sec continuous insonation and hemorrhage increased when the time between ultrasound pulses increased [97].

Increased microbubble diameter has also been associated with an increased propensity for the microbubbles to interact with the vessel wall [7, 98–100]. Mechanisms for this increase include the extended lifetime of larger microbubbles. In *ex vivo* rat cecum, bubbles larger than 4 μm were observed to oscillate for 176±139 pulses on average, compared to 31±14 pulses for bubbles smaller than 4 μm (with a transmitted center frequency of 1 MHz, PRP of 800 kPa and 10 cycle pulses)[7]. With this extended lifetime, the large microbubbles can be deflected to the wall by ultrasound radiation force[101, 102]. In addition, assuming the same distance to the wall, the likelihood of a liquid jet increases with a larger microbubble.

Both biological effects and the delivery of a drug from a microbubble increase with increasing dose, particularly since the number of bubbles near boundaries increases with

increased concentration. For a dosage above 1 mL/kg, petechial hemorrhages were reported to increase in proportion to Optison dose in mouse intestine and abdominal muscle [97]. In an *ex vivo* rat cecum, the presence of a high concentration of microbubbles (>20 microbubbles per $(200\text{-}\mu m)^2$ field) resulted in microbubble fusion, with the larger, fused microbubbles interacting with the vessel wall [103].

4.2 Drug delivery applications

Applications of microbubble-enhanced drug delivery are expanding rapidly and include therapeutic delivery to solid tumors[104–107], delivery across the BBB[108]and enhanced transfection efficiency[104, 109, 110] (Table 2). Perhaps the fastest developing application has been the use of ultrasound-microbubble techniques to treat cancer. Recently-published cancer drug delivery strategies include the local delivery of doxorubicin[105], cis-diamminedichloroplatinum (II) (CDDP) [107]and paclitaxel[106]. For example, [105] reported the delivery of ~9 % of the injected dose of doxorubicin per cubic centimeter to tumors in a rat model with significant therapeutic improvement with the addition of ultrasound. Other reported strategies include the delivery of herpes simplex virus thymidine kinase (TK) and ganciclovir[104], and the delivery of exogenous antigens into the cytosol of dendritic cells[111].

Applications of ultrasound to enhance drug pharmacokinetics and distribution include the treatment of kidney disease [108]and the delivery of an anti-A beta antibody to the brain [112]. Enhancing delivery across tight endothelial junctions, such as those present within the blood-brain barrier, is one of the most important applications of ultrasound-enhanced delivery, since it represents one of few feasible approaches[94, 112]. Applications of gene therapy with microbubble-enhanced transfection include the treatment of diabetes, cardiovascular disease, peripheral vascular disease and regenerative medicine[104, 109, 110, 113, 114]. Finally, microbubble based delivery has been proposed as method to deposit surgical tattoos and thus enhance the efficacy of surgical resection[115].

5.0 Summary

There are many exciting opportunities to leverage ultrasound contrast agents and molecular imaging in the development of new therapeutic strategies. Those emphasized here include the use of ligand-conjugated microbubbles to detect vascular receptors and thus individualize therapy, the use of ultrasound flow mapping to characterize the anti-vascular effect of various therapies and the use of microbubbles to enhance drug and gene delivery.

At this time, a targeted microbubble agent from Bracco (BR55) is reported to be approaching clinical evaluation and strategies for imaging targeted agents are available on commercial ultrasound scanners[118]. Preclinically-formulated targeted microbubbles are widely available and the imaging of such agents to monitor therapy is widespread. Methods to quantify accumulation are advancing, facilitating longitudinal studies. As described here, such agents can be insonified at a low acoustic pressure and high ultrasound frequency and under such conditions the safety profile is optimized.

The use of ultrasound with microbubbles to enhance drug delivery is now frequently reported in pre-clinical research; however, planning for clinical studies is still underway. Optimization of ultrasound-enhanced drug or gene delivery vehicles is challenging due to wide range of possible ultrasound parameters and the range of potential materials, targeting ligands, and cargos. The use of cross-modality validation methods has increased with nuclear medicine, MRI and optical imaging probes used to image the delivery vehicle or the model drug [119–122]. PET provides real-time and highly sensitive full-body pharmacokinetics [113, 122, 123]. MRI can be used to visualize the biodistribution of drugs

or vehicles [120] and the activation of delivery vehicles [119]. Optical imaging can validate the accumulation of targeted microbubbles or drugs [40, 76]. Validation tools are important for the optimization of and the translation of microbubble-based techniques to the clinic.

The optimization of methods to quantify and characterize drug accumulation is particularly critical and timely. In particular, high pressure and low frequency insonation of microbubbles within the vasculature has been shown to alter local blood flow and angiogenesis. Thus, drug accumulation within the altered vasculature may result but may not fully treat the surrounding tumor. Thus, measurement of accumulation within and outside the vasculature during and after insonation will be an important component of system optimization.

References

1. Klibanov AL. Ligand-carrying gas-filled microbubbles: Ultrasound contrast agents for targeted molecular imaging. Bioconjugate Chemistry. Jan-Feb.2005 16:9–17. [PubMed: 15656569]
2. Lum AFH, Borden MA, Dayton PA, Kruse DE, Simon SI, Ferrara KW. Ultrasound radiation force enables targeted deposition of model drug carriers loaded on microbubbles. Journal of Controlled Release. Mar 10.2006 111:128–134. [PubMed: 16380187]
3. Serfis AB, Katzenberger R, Williams K, Tran N. Association of blood clotting factors I and VII with phospholipid monolayers at the air-water interface. Journal of Colloid and Interface Science. Jul. 1999 215:356–363. [PubMed: 10419671]
4. Morgan KE, Allen JS, Dayton PA, Chomas JE, Klibanov AL, Ferrara KW. Experimental and theoretical evaluation of microbubble behavior: Effect of transmitted phase and bubble size. Ieee Transactions on Ultrasonics Ferroelectrics and Frequency Control. Nov.2000 47:1494–1509.
5. Chomas JE, Dayton PA, May D, Allen J, Klibanov A, Ferrara K. Optical observation of contrast agent destruction. Applied Physics Letters. Aug.2000 77:1056–1058.
6. Meijering BD, Juffermans LJ, van Wamel A, Henning RH, Zuhorn IS, Emmer M, Versteilen AM, Paulus WJ, van Gilst WH, Kooiman K, de Jong N, Musters RJ, Deelman LE, Kamp O. Ultrasound and microbubble-targeted delivery of macromolecules is regulated by induction of endocytosis and pore formation. Circ Res. Mar 13.2009 104:679–87. [PubMed: 19168443]
7. Caskey CF, Stieger SM, Qin S, Dayton PA, Ferrara KW. Direct observations of ultrasound microbubble contrast agent interaction with the microvessel wall. Journal of the Acoustical Society of America. Aug.2007 122:1191–1200. [PubMed: 17672665]
8. Qin S, Caskey CF, Ferrara KW. Ultrasound contrast microbubbles in imaging and therapy: physical principles and engineering. Phys Med Biol. Mar 21; 2009 54(6):R27–57. [PubMed: 19229096]
9. Klein C, Nekolla SG, Bengel FM, Momose M, Sammer A, Haas F, Schnackenburg B, Delius W, Mudra H, Wolfram D, Schwaiger M. Assessment of myocardial viability with contrast-enhanced magnetic resonance imaging: comparison with positron emission tomography. Circulation. Jan 15.2002 105:162–7. [PubMed: 11790695]
10. Wagner A, Mahrholdt H, Holly TA, Elliott MD, Regenfus M, Parker M, Klocke FJ, Bonow RO, Kim RJ, Judd RM. Contrast-enhanced MRI and routine single photon emission computed tomography (SPECT) perfusion imaging for detection of subendocardial myocardial infarcts: an imaging study. Lancet. Feb 1.2003 361:374–9. [PubMed: 12573373]
11. Miller JC, Pien HH, Sahani D, Sorensen AG, Thrall JH. Imaging angiogenesis: applications and potential for drug development. J Natl Cancer Inst. Feb 2.2005 97:172–87. [PubMed: 15687360]
12. Paul AK, Nabi HA. Gated myocardial perfusion SPECT: basic principles, technical aspects, and clinical applications. J Nucl Med Technol. Dec.2004 32:179–87. quiz 188–9. [PubMed: 15576339]
13. Padhani AR, Husband JE. Dynamic contrast-enhanced MRI studies in oncology with an emphasis on quantification, validation and human studies. Clin Radiol. Aug.2001 56:607–20. [PubMed: 11467863]
14. Schwitter J, Nanz D, Kneifel S, Bertschinger K, Buchi M, Knusel PR, Marincek B, Luscher TF, von Schulthess GK. Assessment of myocardial perfusion in coronary artery disease by magnetic

resonance: a comparison with positron emission tomography and coronary angiography. Circulation. May 8.2001 103:2230–5. [PubMed: 11342469]

15. Phillips PJ. Contrast pulse sequences (CPS): imaging nonlinear microbubbles. Ultrasonics Symposium, 2001 IEEE. 2001; 2:1739–1745 .
16. Burns PN, Wilson SR, Simpson DH. Pulse inversion imaging of liver blood flow: improved method for characterizing focal masses with microbubble contrast. Invest Radiol. Jan.2000 35:58–71. [PubMed: 10639037]
17. Needles A, Mehi J, Arditi M, Gaud E, Frinking P, Rognin N, Hirson D, Foster FS. Nonlinear contrast agent imaging with a linear array based micro-ultrasound system. Ultrasonics Symposium (IUS), 2009 IEEE International. 2009:279–282.
18. Wei K, Jayaweera AR, Firoozan S, Linka A, Skyba DM, Kaul S. Quantification of myocardial blood flow with ultrasound-induced destruction of microbubbles administered as a constant venous infusion. Circulation. Feb 10.1998 97:473–83. [PubMed: 9490243]
19. Toledo E, Jacobs LD, Lodato JA, DeCara JM, Coon P, Mor-Avi V, Lang RM. Quantitative diagnosis of stress-induced myocardial ischemia using analysis of contrast echocardiographic parametric perfusion images. Eur J Echocardiogr. Jun.2006 7:217–25. [PubMed: 16157510]
20. Yano A, Ito H, Iwakura K, Kimura R, Tanaka K, Okamura A, Kawano S, Masuyama T, Fujii K. Myocardial contrast echocardiography with a new calibration method can estimate myocardial viability in patients with myocardial infarction. J Am Coll Cardiol. May 19.2004 43:1799–806. [PubMed: 15145103]
21. Yu EH, Skyba DM, Leong-Poi H, Sloggett C, Jamorski M, Garg R, Iwanochko RM, Siu SC. Incremental value of parametric quantitative assessment of myocardial perfusion by triggered Low-Power myocardial contrast echocardiography. J Am Coll Cardiol. May 19.2004 43:1807–13. [PubMed: 15145104]
22. Ellegala DB, Leong-Poi H, Carpenter JE, Klibanov AL, Kaul S, Shaffrey ME, Sklenar J, Lindner JR. Imaging tumor angiogenesis with contrast ultrasound and microbubbles targeted to alpha(v)beta3. Circulation. Jul 22.2003 108:336–41. [PubMed: 12835208]
23. Broillet A, Hantson J, Ruegg C, Messager T, Schneider M. Assessment of microvascular perfusion changes in a rat breast tumor model using SonoVue to monitor the effects of different anti-angiogenic therapies. Acad Radiol. May; 2005 12(Suppl 1):S28–33. [PubMed: 16106543]
24. Wei K, Le E, Bin JP, Coggins M, Thorpe J, Kaul S. Quantification of renal blood flow with contrast-enhanced ultrasound. J Am Coll Cardiol. Mar 15.2001 37:1135–40. [PubMed: 11263620]
25. Lindner JR, Womack L, Barrett EJ, Weltman J, Price W, Harthun NL, Kaul S, Patrie JT. Limb stress-rest perfusion imaging with contrast ultrasound for the assessment of peripheral arterial disease severity. JACC Cardiovasc Imaging. May.2008 1:343–50. [PubMed: 19356447]
26. Krix M, Plathow C, Kiessling F, Herth F, Karcher A, Essig M, Schmitteckert H, Kauczor HU, Delorme S. Quantification of perfusion of liver tissue and metastases using a multivessel model for replenishment kinetics of ultrasound contrast agents. Ultrasound Med Biol. Oct.2004 30:1355–63. [PubMed: 15582235]
27. Chomas JE, Pollard RE, Sadlowski AR, Griffey SM, Wisner ER, Ferrara KW. Contrast-enhanced US of microcirculation of superficially implanted tumors in rats. Radiology. Nov.2003 229:439–46. [PubMed: 14526091]
28. Sugimoto K, Moriyasu F, Kamiyama N, Metoki R, Iijima H. Parametric imaging of contrast ultrasound for the evaluation of neovascularization in liver tumors. Hepatol Res. Jun.2007 37:464–72. [PubMed: 17539818]
29. Pollard RE, Dayton PA, Watson KD, Hu X, Guracar IM, Ferrara KW. Motion corrected cadence CPS ultrasound for quantifying response to vasoactive drugs in a rat kidney model. Urology. Sep. 2009 74:675–81. [PubMed: 19589583]
30. Pollard RE, Sadlowski AR, Bloch SH, Murray L, Wisner ER, Griffey S, Ferrara KW. Contrast-assisted destruction-replenishment ultrasound for the assessment of tumor microvasculature in a rat model. Technol Cancer Res Treat. Dec.2002 1:459–70. [PubMed: 12625773]
31. Hu-Lowe DD, Chen E, Zhang L, Watson KD, Mancuso P, Lappin P, Wickman G, Chen JH, Wang J, Jiang X, Amundson K, Simon R, Erbersdobler A, Bergqvist S, Feng Z, Swanson TA, Simmons BH, Lippincott J, Casperson GF, Levin WJ, Stampino CG, Shalinsky DR, Ferrara KW, Fiedler W,

Bertolini F. Targeting Activin Receptor-Like Kinase 1 Inhibits Angiogenesis and Tumorigenesis through a Mechanism of Action Complementary to Anti-VEGF Therapies. Cancer Res. Feb 15.2011 71:1362–1373. [PubMed: 21212415]

32. Watson K, Hu X, Lai C, Lindfors H, Hu-Lowe D, Tuthill T, Shalinsky D, Ferrara K. Novel Ultrasound and DCE-MRI Analyses after Antiangiogenic Treatment with a Selective VEGF Receptor Inhibitor. Ultrasound in Medicine & Biology. 2011
33. Lassau N, Chami L, Benatsou B, Peronneau P, Roche A. Dynamic contrast-enhanced ultrasonography (DCE-US) with quantification of tumor perfusion: a new diagnostic tool to evaluate the early effects of antiangiogenic treatment. Eur Radiol. Dec; 2007 17(Suppl 6):F89–98. [PubMed: 18376462]
34. Lassau N, Chebil M, Chami L, Bidault S, Girard E, Roche A. Dynamic contrast-enhanced ultrasonography (DCE-US): a new tool for the early evaluation of antiangiogenic treatment. Target Oncol. Mar.2010 5:53–8. [PubMed: 20379790]
35. Wiesmann M, Meyer K, Albers T, Seidel G. Parametric perfusion imaging with contrast enhanced ultrasound in acute ischemic stroke. Stroke. Feb.2004 35:508–13. [PubMed: 14739406]
36. Wiesmann M, Seidel G. Ultrasound perfusion imaging of the human brain. Stroke. Oct.2000 31:2421–5. [PubMed: 11022074]
37. Vicenzini E, Delfini R, Magri F, Puccinelli F, Altieri M, Santoro A, Giannoni MF, Bozzao L, Di Piero V, Lenzi GL. Semiquantitative human cerebral perfusion assessment with ultrasound in brain space-occupying lesions: preliminary data. J Ultrasound Med. May.2008 27:685–92. [PubMed: 18424642]
38. Seo JW, Zhang H, Kukis DL, Meares CF, Ferrara KW. A Novel Method to Label Preformed Liposomes with (CU)-C-64 for Positron Emission Tomography (PET) Imaging. Bioconjugate Chemistry. Dec.2008 19:2577–2584. [PubMed: 18991368]
39. Bloch SH, Dayton PA, Ferrara KW. Targeted imaging using ultrasound contrast agents. Progess and opportunities for clinical and research applications. IEEE Eng Med Biol Mag. Sep-Oct.2004 23:18–29. [PubMed: 15565796]
40. Anderson CR, Hu X, Zhang H, Tlaxca J, Decleves AE, Houghtaling R, Sharma K, Lawrence M, Ferrara KW, Rychak JJ. Ultrasound molecular imaging of tumor angiogenesis with an integrin targeted microbubble contrast agent. Invest Radiol. Apr.2011 46:215–24. [PubMed: 21343825]
41. Zhao S, Kruse DE, Ferrara KW, Dayton PA. Selective imaging of adherent targeted ultrasound contrast agents. Phys Med Biol. Apr 21.2007 52:2055–72. [PubMed: 17404455]
42. Hu X, Zheng H, Kruse DE, Sutcliffe P, Stephens DN, Ferrara KW. A sensitive TLRH targeted imaging technique for ultrasonic molecular imaging. IEEE Trans Ultrason Ferroelectr Freq Control. 2010; 57:305–16. [PubMed: 20178897]
43. Miller DL, Dou C, Wiggins RC. Frequency dependence of kidney injury induced by contrast-aided diagnostic ultrasound in rats. Ultrasound Med Biol. May 14.2008
44. Korpanty G, Carbon JG, Grayburn PA, Fleming JB, Brekken RA. Monitoring response to anticancer therapy by targeting microbubbles to tumor vasculature. Clin Cancer Res. Jan 1.2007 13:323–30. [PubMed: 17200371]
45. Ley K, Laudanna C, Cybulsky MI, Nourshargh S. Getting to the site of inflammation: the leukocyte adhesion cascade updated. Nat Rev Immunol. Sep.2007 7:678–89. [PubMed: 17717539]
46. Carmeliet P, Jain RK. Angiogenesis in cancer and other diseases. Nature. 2000; 407:249–257. [PubMed: 11001068]
47. Heinemann V, Hoff PM. Bevacizumab plus irinotecan-based regimens in the treatment of metastatic colorectal cancer. Oncology. 2010; 79:118–28. [PubMed: 21088438]
48. Pochon S, Tardy I, Bussat P, Bettinger T, Brochot J, von Wronski M, Passantino L, Schneider M. BR55: A Lipopeptide-Based VEGFR2-Targeted Ultrasound Contrast Agent for Molecular Imaging of Angiogenesis. Investigative Radiology. 2010; 45:89–95.10.1097/RLI. 0b013e3181c5927c [PubMed: 20027118]
49. Willmann JK, Kimura RH, Deshpande N, Lutz AM, Cochran JR, Gambhir SS. Targeted Contrast-Enhanced Ultrasound Imaging of Tumor Angiogenesis with Contrast Microbubbles Conjugated to Integrin-Binding Knottin Peptides. J Nucl Med. March 1.2010 51:433–440. [PubMed: 20150258]

50. Jun HY, Park SH, Kim HS, Yoon K-H. Long Residence Time of Ultrasound Microbubbles Targeted to Integrin in Murine Tumor Model. Academic Radiology. 2010; 17:54–60. [PubMed: 19815430]
51. Anderson CR, Rychak JJ, Backer M, Backer J, Ley K, Klibanov AL. scVEGF Microbubble Ultrasound Contrast Agents: A Novel Probe for Ultrasound Molecular Imaging of Tumor Angiogenesis. Investigative Radiology. 2010; 45:579–585.10.1097/RLI.0b013e3181efd581 [PubMed: 20733505]
52. Lee DJ, Lyshchik A, Huamani J, Hallahan DE, Fleischer AC. Relationship Between Retention of a Vascular Endothelial Growth Factor Receptor 2 (VEGFR2)-Targeted Ultrasonographic Contrast Agent and the Level of VEGFR2 Expression in an In Vivo Breast Cancer Model. J Ultrasound Med. June 1.2008 27:855–866. [PubMed: 18499845]
53. Willmann JK, Lutz AM, Paulmurugan R, Patel MR, Chu P, Rosenberg J, Gambhir SS. Dual-targeted contrast agent for US assessment of tumor angiogenesis in vivo. Radiology. Sep.2008 248:936–44. [PubMed: 18710985]
54. Deshpande N, Ren Y, Foygel K, Rosenberg J, Willmann K Jr. Tumor Angiogenic Marker Expression Levels during Tumor Growth: Longitudinal Assessment with Molecularly Targeted Microbubbles and US Imaging. Radiology. March 1.2011 258:804–811. [PubMed: 21339349]
55. Leong-Poi H, Christiansen J, Klibanov AL, Kaul S, Lindner JR. Noninvasive Assessment of Angiogenesis by Ultrasound and Microbubbles Targeted to {alpha}v-Integrins. Circulation. January 28.2003 107:455–460. [PubMed: 12551871]
56. Stieger SM, Dayton PA, Borden MA, Caskey CF, Griffey SM, Wisner ER, Ferrara KW. Imaging of angiogenesis using Cadence contrast pulse sequencing and targeted contrast agents. Contrast Media Mol Imaging. Jan.2008 3:9–18. [PubMed: 18335479]
57. Korpanty G, Chen S, Shohet RV, Ding J, Yang B, Frenkel PA, Grayburn PA. Targeting of VEGF-mediated angiogenesis to rat myocardium using ultrasonic destruction of microbubbles. Gene Ther. Sep.2005 12:1305–12. [PubMed: 15829992]
58. Palmowski M, Huppert J, Ladewig G, Hauff P, Reinhardt M, Mueller MM, Woenne EC, Jenne JW, Maurer M, Kauffmann GW, Semmler W, Kiessling F. Molecular profiling of angiogenesis with targeted ultrasound imaging: early assessment of antiangiogenic therapy effects. Mol Cancer Ther. Jan.2008 7:101–9. [PubMed: 18202013]
59. Guenther F, von zur Muhlen C, Ferrante EA, Grundmann S, Bode C, Klibanov AL. An ultrasound contrast agent targeted to P-selectin detects activated platelets at supra-arterial shear flow conditions. Invest Radiol. Oct.2010 45:586–91. [PubMed: 20808239]
60. Ferrante EA, Pickard JE, Rychak J, Klibanov A, Ley K. Dual targeting improves microbubble contrast agent adhesion to VCAM-1 and P-selectin under flow. Journal of Controlled Release. 2009; 140:100–107. [PubMed: 19666063]
61. Kaufmann BA, Sanders JM, Davis C, Xie A, Aldred P, Sarembock IJ, Lindner JR. Molecular imaging of inflammation in atherosclerosis with targeted ultrasound detection of vascular cell adhesion molecule-1. Circulation. Jul 17.2007 116:276–84. [PubMed: 17592078]
62. Klibanov AL, Rychak JJ, Yang WC, Alikhani S, Li B, Acton S, Lindner JR, Ley K, Kaul S. Targeted ultrasound contrast agent for molecular imaging of inflammation in high-shear flow. Contrast Media & Molecular Imaging. 2006; 1:259–266. [PubMed: 17191766]
63. Takalkar AM, Klibanov AL, Rychak JJ, Lindner JR, Ley K. Binding and detachment dynamics of microbubbles targeted to P-selectin under controlled shear flow. Journal of Controlled Release. 2004; 96:473–482. [PubMed: 15120903]
64. Kaufmann BA, Carr CL, Belcik JT, Xie A, Yue Q, Chadderdon S, Caplan ES, Khangura J, Bullens S, Bunting S, Lindner JR. Molecular Imaging of the Initial Inflammatory Response in Atherosclerosis: Implications for Early Detection of Disease. Arterioscler Thromb Vasc Biol. January 1.2010 30:54–59. [PubMed: 19834105]
65. Villanueva FS, Lu E, Bowry S, Kilic S, Tom E, Wang J, Gretton J, Pacella JJ, Wagner WR. Myocardial ischemic memory imaging with molecular echocardiography. Circulation. Jan 23.2007 115:345–52. [PubMed: 17210843]

66. Kaufmann BA, Lewis C, Xie A, Mirza-Mohd A, Lindner JR. Detection of recent myocardial ischaemia by molecular imaging of P-selectin with targeted contrast echocardiography. Eur Heart J. Aug.2007 28:2011–7. [PubMed: 17526905]

67. Krieglstein CF, Granger DN. Adhesion molecules and their role in vascular disease. American Journal of Hypertension. 2001; 14:S44–S54.

68. Lindner JR, Song J, Xu F, Klibanov AL, Singbartl K, Ley K, Kaul S. Noninvasive ultrasound imaging of inflammation using microbubbles targeted to activated leukocytes. Circulation. Nov 28.2000 102:2745–50. [PubMed: 11094042]

69. Bachmann C, Klibanov AL, Olson TS, Sonnenschein JR, Rivera-Nieves J, Cominelli F, Ley KF, Lindner JR, Pizarro TT. Targeting mucosal addressin cellular adhesion molecule (MAdCAM)-1 to noninvasively image experimental Crohn's disease. Gastroenterology. Jan.2006 130:8–16. [PubMed: 16401463]

70. Schumann PA, Christiansen JP, Quigley RM, McCreery TP, Sweitzer RH, Unger EC, Lindner JR, Matsunaga TO. Targeted-microbubble binding selectively to GPIIb III a receptors of platelet thrombi. Invest Radiol. Nov.2002 37:587–93. [PubMed: 12393970]

71. Weller GER, Lu E, Csikari MM, Klibanov AL, Fischer D, Wagner WR, Villanueva FS. Ultrasound Imaging of Acute Cardiac Transplant Rejection With Microbubbles Targeted to Intercellular Adhesion Molecule-1. Circulation. July 15.2003 108:218–224. [PubMed: 12835214]

72. Ferrara K, Pollard R, Borden M. Ultrasound microbubble contrast agents: Fundamentals and application to gene and drug delivery. Annual Review of Biomedical Engineering. 2007; 9:415–447.

73. Ferrara KW. Driving delivery vehicles with ultrasound. Advanced Drug Delivery Reviews. Jun. 2008 60:1097–1102. [PubMed: 18479775]

74. Ferrara KW, Borden MA, Zhang H. Lipid-Shelled Vehicles: Engineering for Ultrasound Molecular Imaging and Drug Delivery. Accounts of Chemical Research. Jul.2009 42:881–892. [PubMed: 19552457]

75. Miller DL, Quddus J. Diagnostic ultrasound activation of contrast agent gas bodies induces capillary rupture in mice. Proceedings Of The National Academy Of Sciences Of The United States Of America. Aug.2000 97:10179–10184. [PubMed: 10954753]

76. Price RJ, Skyba DM, Kaul S, Skalak TC. Delivery of colloidal particles and red blood cells to tissue through microvessel ruptures created by targeted microbubble destruction with ultrasound. Circulation. Sep 29.1998 98:1264–7. [PubMed: 9751673]

77. Lentacker I, Geers B, Demeester J, De Smedt SC, Sanders NN. Design and evaluation of doxorubicin-containing microbubbles for ultrasound-triggered doxorubicin delivery: cytotoxicity and mechanisms involved. Mol Ther. Jan.2010 18:101–8. [PubMed: 19623162]

78. Christiansen JP, French BA, Klibanov AL, Kaul S, Lindner JR. Targeted tissue transfection with ultrasound destruction of plasmid-bearing cationic microbubbles. Ultrasound in Medicine and Biology. Dec.2003 29:1759–1767. [PubMed: 14698343]

79. Hauff P, Seemann S, Reszka R, Schultze-Mosgau M, Reinhardt M, Buzasi T, Plath T, Rosewicz S, Schirner M. Evaluation of gas-filled microparticles and sonoporation as gene delivery system: feasibility study in rodent tumor models. Radiology. Aug.2005 236:572–8. [PubMed: 16040915]

80. Tartis MS, McCallan J, Lum AF, Labell R, Stieger SM, Matsunaga TO, Ferrara KW. Therapeutic effects of paclitaxel-containing ultrasound contrast agents. Ultrasound Med Biol. Nov.2006 32:1771–80. [PubMed: 17112963]

81. Kooiman K, Bohmer MR, Emmer M, Vos HJ, Chlon C, Shi WT, Hall CS, de Winter S, Schroen K, Versluis M, de Jong N, van Wamel A. Oil-filled polymer microcapsules for ultrasound-mediated delivery of lipophilic drugs. Journal of Controlled Release. Jan.2009 133:109–118. [PubMed: 18951931]

82. Kheirolomoom A, Dayton PA, Lum AFH, Little E, Paoli EE, Zheng H, Ferrara KW. Acoustically-active microbubbles conjugated to liposomes: Characterization of a proposed drug delivery vehicle. Journal of Controlled Release. 2007; 118:275–284. [PubMed: 17300849]

83. Frenkel PA, Chen SY, Thai T, Shohet RV, Grayburn PA. DNA-loaded albumin microbubbles enhance ultrasound-mediated transfection in vitro. Ultrasound in Medicine and Biology. Jun.2002 28:817–822. [PubMed: 12113794]

84. Lentacker I, De Geest BG, Vandenbroucke RE, Peeters L, Demeester J, De Smedt SC, Sanders NN. Ultrasound-responsive polymer-coated microbubbles that bind and protect DNA. Langmuir. Aug 15.2006 22:7273–7278. [PubMed: 16893226]

85. Borden MA, Caskey CF, Little E, Gillies RJ, Ferrara KW. DNA and polylysine adsorption and multilayer construction onto cationic lipid-coated microbubbles. Langmuir. 2007; 23:9401–9408. [PubMed: 17665937]

86. Stieger SM, Caskey CF, Adamson RH, Qin S, Curry FR, Wisner ER, Ferrara KW. Enhancement of vascular permeability with low-frequency contrast-enhanced ultrasound in the chorioallantoic membrane model. Radiology. Apr.2007 243:112–21. [PubMed: 17392250]

87. Lanza GM, Wallace KD, Fischer SE, Christy DH, Scott MJ, Trousil RL, Cacheris WP, Miller JG, Gaffney PJ, Wickline SA. High-frequency ultrasonic detection of thrombi with a targeted contrast system. Ultrasound Med Biol. 1997; 23:863–70. [PubMed: 9300990]

88. Lanza GM, Wallace KD, Scott MJ, Cacheris WP, Abendschein DR, Christy DH, Sharkey AM, Miller JG, Gaffney PJ, Wickline SA. A novel site-targeted ultrasonic contrast agent with broad biomedical application. Circulation. Dec.1996 94:3334–3340. [PubMed: 8989148]

89. Dayton PA, Zhao SK, Bloch SH, Schumann P, Penrose K, Matsunaga TO, Zutshi R, Doinikov A, Ferrara KW. Application of ultrasound to selectively localize nanodroplets for targeted imaging and therapy. Molecular Imaging. Jul.2006 5:160–174. [PubMed: 16954031]

90. Rapoport N, Gao ZG, Kennedy A. Multifunctional nanoparticles for combining ultrasonic tumor imaging and targeted chemotherapy. Journal of the National Cancer Institute. Jul.2007 99:1095–1106. [PubMed: 17623798]

91. Meltzer RS. Food and Drug Administration ultrasound device regulation: The output display standard, the “mechanical index. and ultrasound safety,” Journal of the American Society of Echocardiography. 1996; 9:216–220.

92. Frizzell LA, Chen E, Lee C. Effects of pulsed ultrasound on the mouse neonate: hind limb paralysis and lung hemorrhage. Ultrasound Med Biol. 1994; 20:53–63. [PubMed: 8197627]

93. Qin SP, Ferrara KW. Acoustic response of compliable microvessels containing ultrasound contrast agents. Physics in Medicine and Biology. 2006; 51:5065–5088. [PubMed: 17019026]

94. Mcdannold N, Vykhodtseva N, Hynynen K. Effects of acoustic parameters and ultrasound contrast agent dose on focused-ultrasound induced blood-brain barrier disruption. Ultrasound in Medicine and Biology. Jun.2008 34:930–937. [PubMed: 18294757]

95. Caskey CF, Qin SP, Dayton PA, Ferrara KW. Microbubble tunneling in gel phantoms. Journal of the Acoustical Society of America. May.2009 125:EL183–EL189. [PubMed: 19425620]

96. Wible JH, Galen KP Jr, Wojdyla JK, Hughes MS, Klibanov AL, Brandenburger GH. Microbubbles induce renal hemorrhage when exposed to diagnostic ultrasound in anesthetized rats. Ultrasound Med Biol. Nov–Dec.2002 28:1535–46. [PubMed: 12498949]

97. Miller DL, Quddus J. Diagnostic ultrasound activation of contrast agent gas bodies induces capillary rupture in mice. Proc Natl Acad Sci U S A. Aug 29.2000 97:10179–84. [PubMed: 10954753]

98. Pislaru SV, Pislaru C, Kinnick RR, Singh R, Gulati R, Greenleaf JF, Simari RD. Optimization of ultrasound-mediated gene transfer: comparison of contrast agents and ultrasound modalities. Eur Heart J. Sep.2003 24:1690–8. [PubMed: 14499233]

99. Miller DL, Gies RA. The influence of ultrasound frequency and gas-body composition on the contrast agent-mediated enhancement of vascular bioeffects in mouse intestine. Ultrasound Med Biol. Feb.2000 26:307–13. [PubMed: 10722920]

100. Choi JJ, Feshitan JA, Baseri B, Shougang W, Yao-Sheng T, Borden MA, Konofagou EE. Microbubble-Size Dependence of Focused Ultrasound-Induced Blood–Brain Barrier Opening in Mice In Vivo. Biomedical Engineering, IEEE Transactions on. 2010; 57:145–154.

101. Dayton PA, Allen JS, Ferrara KW. The magnitude of radiation force on ultrasound contrast agents. Journal of the Acoustical Society of America. Nov.2002 112:2183–2192. [PubMed: 12430830]

102. Dayton PA, Morgan KE, Klibanov ALS, Brandenburger G, Nightingale KR, Ferrara KW. A preliminary evaluation of the effects of primary and secondary radiation forces on acoustic

contrast agents. Ieee Transactions on Ultrasonics Ferroelectrics and Frequency Control. Nov. 1997 44:1264–1277.

103. Zheng HR, Dayton PA, Caskey C, Zhao SK, Qin SP, Ferrara KW. Ultrasound-driven microbubble oscillation and translation within small phantom vessels. Ultrasound in Medicine and Biology. Dec.2007 33:1978–1987. [PubMed: 17900793]
104. Carson AR, McTiernan CF, Lavery L, Hodnick A, Grata M, Leng XP, Wang JJ, Chen XC, Modzelewski RA, Villanueva FS. Gene therapy of carcinoma using ultrasound-targeted microbubble destruction. Ultrasound in Medicine and Biology. Mar.2011 37:393–402. [PubMed: 21256666]
105. Tinkov S, Coester C, Serba S, Geis NA, Katus HA, Winter G, Bekeredjian R. New doxorubicin-loaded phospholipid microbubbles for targeted tumor therapy: In-vivo characterization. Journal of Controlled Release. Dec.2010 148:368–372. [PubMed: 20868711]
106. Rapoport N, Kennedy AM, Shea JE, Scaife CL, Nam KH. Ultrasonic Nanotherapy of Pancreatic Cancer: Lessons from Ultrasound Imaging. Molecular Pharmaceutics. Jan-Feb.2010 7:22–31. [PubMed: 19899813]
107. Watanabe Y, Aoi A, Horie S, Tomita N, Mori S, Morikawa H, Matsumura Y, Vassaux G, Kodama T. Low-intensity ultrasound and microbubbles enhance the antitumor effect of cisplatin. Cancer Science. Dec.2008 99:2525–2531. [PubMed: 19018767]
108. Deelman LE, Decleves AE, Rychak JJ, Sharma K. Targeted renal therapies through microbubbles and ultrasound. Advanced Drug Delivery Reviews. Nov.2010 62:1369–1377. [PubMed: 20946925]
109. Otani K, Yamahara K, Ohnishi S, Obata H, Kitamura S, Nagaya N. Nonviral delivery of siRNA into mesenchymal stem cells by a combination of ultrasound and microbubbles. Journal of Controlled Release. Jan.2009 133:146–153. [PubMed: 18976686]
110. Fujii H, Sun Z, Li SH, Wu J, Fazel S, Weisel RD, Rakowski H, Lindner J, Li RK. Ultrasound-Targeted Gene Delivery Induces Angiogenesis After a Myocardial Infarction in Mice. Jacc-Cardiovascular Imaging. Jul.2009 2:869–879. [PubMed: 19608138]
111. Suzuki R, Oda Y, Utoguchi N, Namai E, Taira Y, Okada N, Kadowaki N, Kodama T, Tachibana K, Maruyama K. A novel strategy utilizing ultrasound for antigen delivery in dendritic cell-based cancer immunotherapy. Journal of Controlled Release. Feb.2009 133:198–205. [PubMed: 19000727]
112. Jordao JF, Ayala-Grosso CA, Markham K, Huang YX, Chopra R, McLaurin J, Hynynen K, Aubert I. Antibodies Targeted to the Brain with Image-Guided Focused Ultrasound Reduces Amyloid-beta Plaque Load in the TgCRND8 Mouse Model of Alzheimer's Disease. Plos One. May.2010 5
113. Watanabe Y, Horie S, Funaki Y, Kikuchi Y, Yamazaki H, Ishii K, Mori S, Vassaux G, Kodama T. Delivery of Na/I Symporter Gene into Skeletal Muscle Using Nanobubbles and Ultrasound: Visualization of Gene Expression by PET. Journal of Nuclear Medicine. Jun.2010 51:951–958. [PubMed: 20484436]
114. Chappell JC, Song J, Burke CW, Klibanov AL, Price RJ. Targeted Delivery of Nanoparticles Bearing Fibroblast Growth Factor-2 by Ultrasonic Microbubble Destruction for Therapeutic Arteriogenesis. Small. Oct.2008 4:1769–1777. [PubMed: 18720443]
115. Couture O, Faivre M, Pannacci N, Babataheri A, Servois V, Tabeling P, Tanter M. Ultrasound internal tattooing. Medical Physics. Feb.2011 38:1116–1123. [PubMed: 21452748]
116. Chen S, Shimoda M, Wang MY, Ding J, Noguchi H, Matsumoto S, Grayburn PA. Regeneration of pancreatic islets in vivo by ultrasound-targeted gene therapy. Gene Therapy. Nov.2010 17:1411–1420. [PubMed: 20508600]
117. Phillips LC, Klibanov AL, Bowles DK, Ragosta M, Hossack JA, Wamhoff BR. Focused in vivo Delivery of Plasmid DNA to the Porcine Vascular Wall via Intravascular Ultrasound Destruction of Microbubbles. Journal of Vascular Research. 2010; 47:270–274. [PubMed: 19923850]
118. Pysz MA, Foygel K, Rosenberg J, Gambhir SS, Schneider M, Willmann K Jr. Antiangiogenic Cancer Therapy: Monitoring with Molecular US and a Clinically Translatable Contrast Agent (BR55)1. Radiology. August 1.2010 256:519–527. [PubMed: 20515975]

119. Ponce AM, Viglianti BL, Yu DH, Yarmolenko PS, Michelich CR, Woo J, Bally MB, Dewhirst MW. Magnetic resonance imaging of temperature-sensitive liposome release: Drug dose painting and antitumor effects. Journal of the National Cancer Institute. Jan.2007 99:53–63. [PubMed: 17202113]

120. Hynynen K, McDannold N. MRI guided and monitored focused ultrasound thermal ablation methods: a review of progress. Int J Hyperthermia. Nov.2004 20:725–37. [PubMed: 15675668]

121. Marik J, Tartis MS, Zhang H, Fung JY, Kheirolomoom A, Sutcliffe JL, Ferrara KW. Long-circulating liposomes radiolabeled with [F-18]fluorodipalmitin ([F-18]FDP). Nuclear Medicine and Biology. Feb.2007 34:165–171. [PubMed: 17307124]

122. Zhang H, Kusunose J, Kheirolomoom A, Seo JW, Qi J, Watson K, Lindfors H, Ruoslahti E, Sutcliffe JL, Ferrara KW. Dynamic imaging of arginine-rich heart-targeted vehicles in a mouse model. Biomaterials. 2008 (in press).

123. Laverman P, Dams ETM, Oyen WJG, Storm G, Koenders EB, Prevost R, van der Meer JWM, Corstens FHM, Boerman OC. A novel method to label liposomes with Tc-99m by the hydrazino nicotinyl derivative. Journal of Nuclear Medicine. 1999; 40:192–197. [PubMed: 9935076]

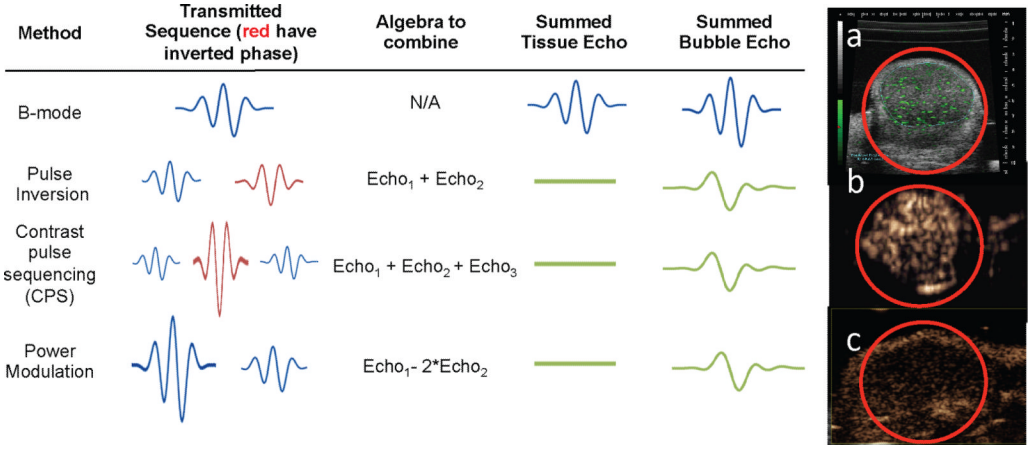

Figure 1. Sample images and methodologies used to distinguish between tissue and microbubble echoes from molecularly targeted agents with clinical (1–15 MHz) and high frequency (20–50 MHz) ultrasound in mouse models of cancer (red circle indicates tumor)

In each case tumors with diameters on the order of 5 mm are displayed. Trains of pulses are applied to the transducer with variations in the phase and amplitude of the pulse. Pulse inversion and power modulation vary only the phase or amplitude of the pulses, respectively, while CPS varies both. Algebraic combinations of these echoes cancel contributions from tissue. (a) High frequency (~40 MHz) image obtained in a linear mode (B-mode) in which the green pixels indicate bound agents and the grey indicates surrounding tissue. Microbubbles were detected based on their entry and accumulation. (b) 7 MHz ultrasound image of bound microbubbles using CPS. Here, the entire image represents microbubble echoes as tissue echoes are efficiently suppressed. (c) High frequency image (~40 MHz) obtained using power modulation. Note the high spatial resolution (compared with b), but the skin line at the top of the image results from reduced tissue cancelation at high frequencies.

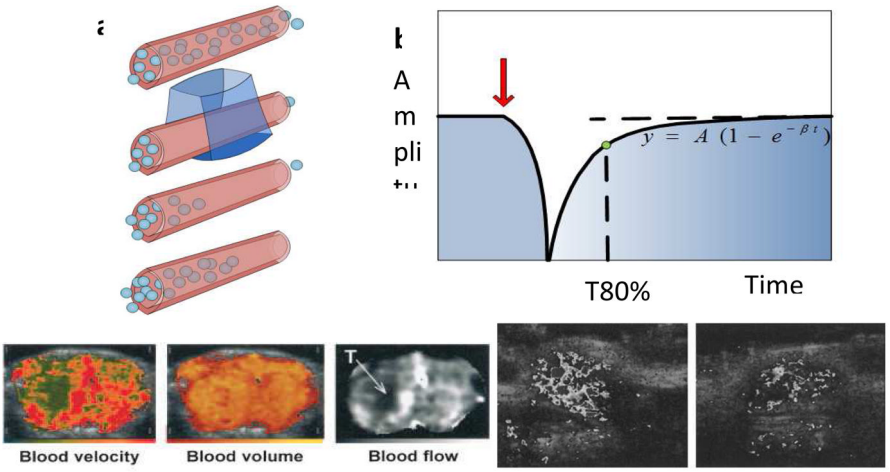

Figure 2. Destruction-replenishment methods for blood flow estimation and applications

After locally fragmenting microbubbles with an ultrasound pulse and imaging their return, the local blood flow rate can be estimated (a). The increasing echo amplitude is modeled as an exponential function (b) and critical parameters, blood velocity (β), blood volume (A) and blood flow (A×β) can be estimated in each pixel. (c–e) The microvascular physiology of a rat glioma tumor (labeled by "T") was depicted by these three parameters (c, d, and e). (f–g) Parametric imaging of blood flow (A×β) was utilized to evaluate rat tumor vasculature after treatment with anti-angiogenic drugs. Compared to the control tumor (f), blood flow in the treated tumor (g) was reduced. (c–e) and (f–g) reproduced with permission from [22] and [23], respectively.

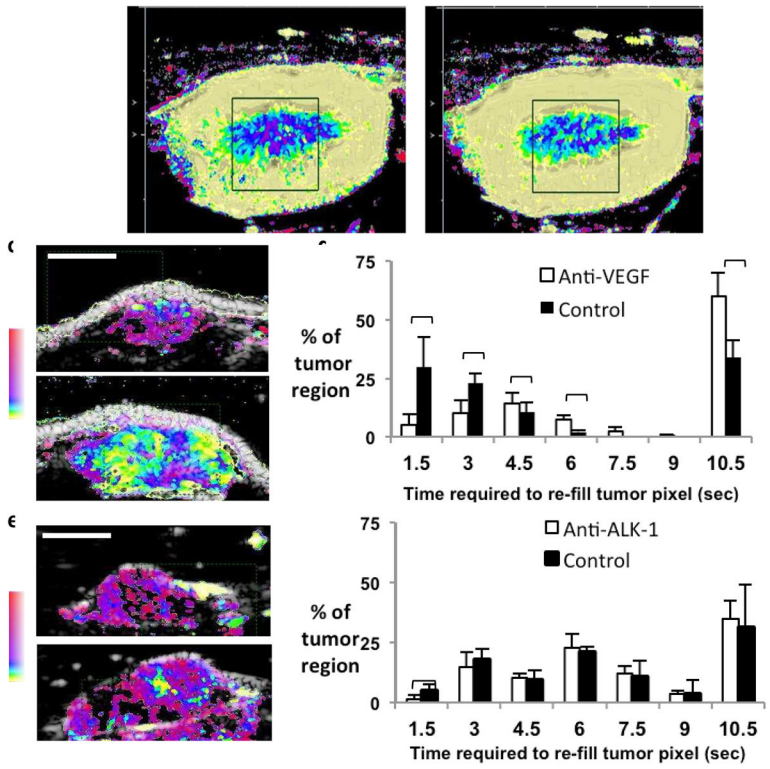

Figure 3. Applications of destruction-replenishment perfusion imaging

The time required for contrast agent replenishment was used to quantify flow in the kidney before (a) and after (b) administration of Dopamine, where yellow indicates fast replenishment (~ 1 second) and pink indicates slow replenishment (10 seconds). As a result of dopamine, the medulla image changes from deep blue to lighter blue indicating a decrease in replenishment time (faster flow) in the kidney. Time for contrast replenishment has also been used to assess the response to anti-angiogenic therapy in rodent tumors. (c–d) Response to anti- VEGF therapy in a rat adenocarcinoma demonstrated that VEGF therapy altered vasculature with fast and slow blood flow. (c) Upper is treated, lower is control. (e–f) Response to anti-ALK-1 therapy in a chimeric mouse model demonstrated that ALK-1 therapy interferes with vascular maturation and influenced flow only in mature vessels with fast flow. (e) The upper frame is ALK-1 treated, lower is diluent treated.

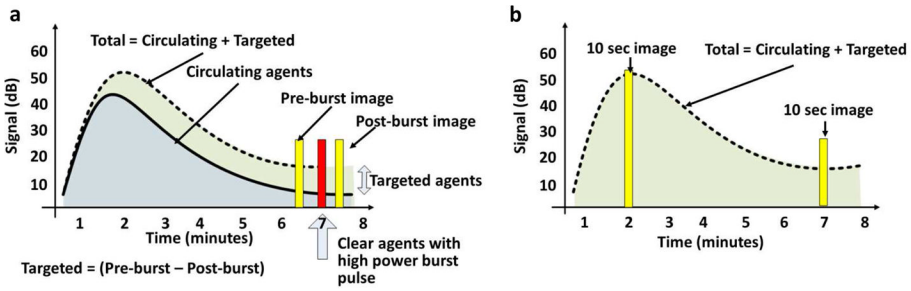

Figure 4. Strategies for the differentiation of bound and circulating microbubbles

In each case, microbubbles are injected and circulate for ~7 minutes. When bound agents are present the image amplitude decays more slowly. (a) Red bar indicates the timing of a high-pressure ultrasound burst to destroy the bound and circulating agents. The pre-burst and post-burst images (yellow bars) are subtracted to yield the targeted agent image. (b) Alternatively, a ten second window of images can be obtained at the time of injection and a later time point (yellow bars), averaging over the ten second interval to suppress the contribution from circulating agents. The late-average image normalized by the early-average image quantifies accumulation.

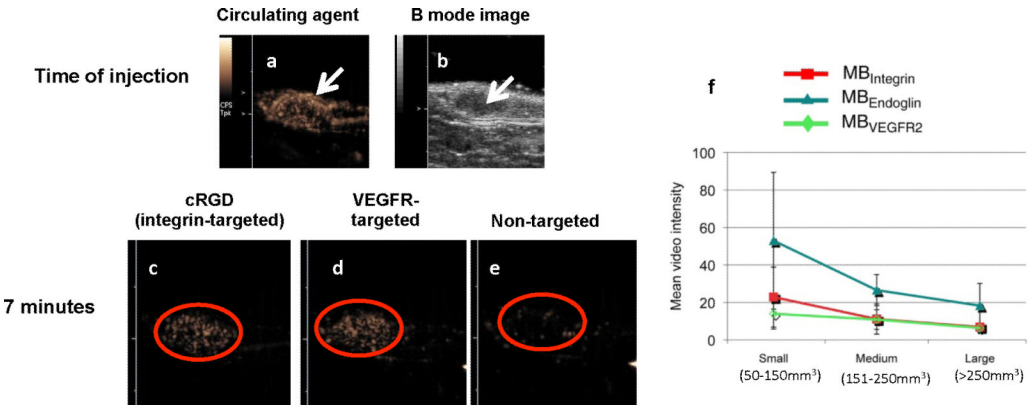

Figure 5. Examples of targeted agents from multiple ligand-receptor pairs obtained with CPS

(a) CPS images of the circulating agent in a Met-1 syngeneic mouse tumor (arrow) immediately after injection and (b) the corresponding B-mode, anatomical image of the tumor region (arrow). Note abundant vasculature in the CPS image. (c–d) cRGD-conjugated [40] and scVEGF-conjugated microbubbles [51] accumulate within the Met-1 tumor to a greater extent than non-targeted microbubbles (e). (f) Mean targeted, contrast-enhanced US imaging signal intensities from longitudinal experiments in subcutaneous ovarian cancer xenografts in mice obtained by using integrin (red), endoglin (teal), and VEGFR2-targeted microbubbles (MB) (green). Absolute and relative US imaging signals were different among different tumor types and different MB types. Error bars = standard deviations.(f) reproduced with permission from [54].

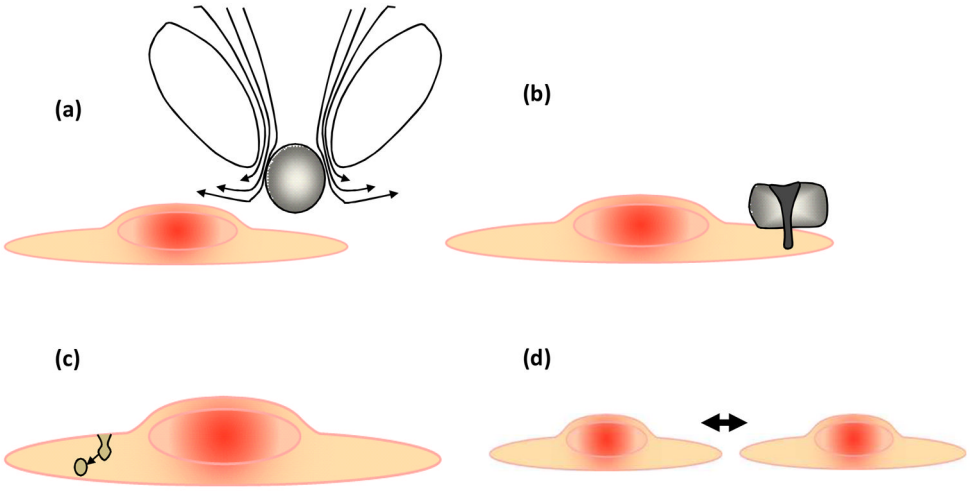

Figure 6. Hypothesized mechanisms for enhanced drug delivery with the insonation of microbubble contrast agents

(a) Fluid microstreaming surrounding an oscillating bubble can enhance transport. (b) Liquid jets create small pores in cell membranes. (c) Ultrasound microbubble oscillation enhances trans-cytosis and (d) increases the width of gaps between endothelial cells.

Table 1

Pre-clinical applications of targeted microbubbles

Clinical Application	Target	Ligand	Tissue Rejection	Bound vs circulating	Ref
Angiogenesis	VEGFR2	Peptide	CPS, clinical freq	Post-burst was negligible	48
	$\alpha_v\beta_3$	Knottin peptide	B-mode, high freq	Pre-burst minus post-burst	49
	$\alpha_v\beta_3$	cRGD	Pulse Inversion, clinical freq	None, video intensity only	50
	VEGFR2	scVEGF	CPS, clinical freq	Pre-burst minus post-burst	51
	$\alpha_v\beta_3$	cRGD	CPS, clinical freq	Pre-burst minus post-burst and Late-average	40
	VEGFR2	antibody vegf	B-mode, high freq	Pre-burst minus post-burst	52
	VEGFR2	anti-vegf and anti-av	B-mode, high freq	Pre-burst minus post-burst	53
	CD105, VEGFR2, VEGF	anti-CD105, anti-VEGFR2, or anti-VEGF-VEGFR complex specific	B-mode, clinical freq	Targeted minus background	44
	$\alpha_v\beta_3$, endoglin, VEGFR2	mAB-alpha(v), mAB-VEGFR2, mAB-endoglin	B-mode, high freq	Pre-burst minus post-burst	54
	alpha(v) integrins	mAB-alpha(v) and RGD-containing echistatin	Doppler, clinical freq	Pre-burst minus post-burst	55
	alpha(v)int egrins	echistatin	CPS, clinical freq	Pre-burst minus post-burst	56
Atherosclerosis	P-selectin	Sialyl Lewis A	N/A	N/A-in vitro	59
	P-Selectin and VCAM-1	mAb-MVCAM.A, a sialyl Lewisx polymer	N/A	N/A-In vitro	60
	VCAM-1	antibody (VCAM-1)	CPS, clinical freq	Pre-burst minus post-burst	61
	P-selectin	sialyl Lewis X	N/A	N/A-intravital microscopy	62
	P-selectin	antibody	N/A	N/A-In vitro	63
	P-Selectin and VCAM-1	antibody (VCAM-1or P-Selectin)	CPS, clinical freq	Pre-burst minus post-burst	64
Inflammation	Selectins	sialyl Lewis X	CPS, clinical freq	Pre-burst minus post-burst	65
	P-Selectin	antibody	CPS, clinical freq	Pre-burst minus post-burst	66
	Monocyte-derived Cells	phosphatidylserine	Pulse Inversion, clinical freq	Pre-burst minus post-burst	68
	MAdCAM-1	MECA-367antibody	Pulse Inversion, clinical freq	Subtract average background	69
	GPIIb IIIa	peptide CRGDC	B-mode image intensity	N/A	70
	ICAM-1	antibody	T1.3R3.6	Pre-burst minus post-burst	71

Table 2

Examples of recent papers demonstrating the applications in drug delivery

Application	Therapeutic cargo or goal	Reference
Cancer	Chemotherapeutics, gene delivery, immunotherapy	[104–107, 111]
Renal	Modify the size selectivity of the filtration capacity of the kidney	[108]
Brain	Delivery across BBB	[94, 112]
Diabetes/pancreas	Transfect pancreatic β-cells	[116]
Cardiovascular disease	Enhance gene transfection and recruit progenitor cells after myocardial infarction	[110, 117]
Peripheral vascular disease/thrombus	Enhance gene transfection	[113, 114]
Regenerative medicine	Nonviral delivery method of siRNA into MSC	[109]
Surgical guidance	Noninvasively deposit markers under image guidance to help surgeons identify targets for resection	[115]